

Supplementary Materials

Printable high-performance iontronic power source based on osmotic effects

Yanhui Liu^{1,2,#}, Puguang Peng^{1,2,#}, Feiyao Yang¹, Zhong Lin Wang^{1,3,4,*}, Di Wei^{1,5,*}

¹Beijing Institute of Nanoenergy and Nanosystems, Chinese Academy of Sciences, Beijing 101400, China.

²School of Nanoscience and Engineering, University of Chinese Academy of Sciences, Beijing 100049, China.

³Beijing Key Laboratory of Micro-Nano Energy and Sensor, Center for High-Entropy Energy and Systems, Beijing Institute of Nanoenergy and Nanosystems, Chinese Academy of Sciences, Beijing 101400, China.

⁴Guangzhou Institute of Blue Energy, Knowledge City, Guangzhou 510555, Guangdong, China.

⁵Centre for Photonic Devices and Sensors, University of Cambridge, Cambridge CB3 0FA, UK.

[#]Authors contributed equally.

***Correspondence to:** Prof. Zhong Lin Wang and Prof. Di Wei, Beijing Institute of Nanoenergy and Nanosystems, Chinese Academy of Sciences, Yard No. 8, Yangyan East 1st Road, Yanxi Economic Development Zone, Huairou Dist, Beijing 101400, China. E-mail: zhong.wang@mse.gatech.edu; dw344@cam.ac.uk

Note S1: The effective working area of the device.

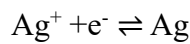
K^+ ions move laterally through the nanoconfined graphene oxide (GO) channels. From **Figure S1a, b**, it can be seen that the graphene oxide (GO) region in the device has a length (L) of 3.92 mm, a width (W) of 2.94 mm, and a height (H) of $\sim 5 \mu\text{m}$. The diffusion cross-sectional area of K^+ ions in the two-dimensional nanoconfined channels can be calculated using the following formula:

$$A = L \times H = 1.96 \times 10^{-6} \text{ m}^2 \#(1)$$

Note S2: The process of estimating the electrode potential of the power source using the Nernst equation.

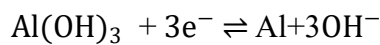
Faradaic reactions are used to enhance the permeation power of ion-electronic devices. The Nernst equation is applied to calculate the electrode potential introduced by the redox reactions. However, since ion-electronic systems are a new type of solid-state power source, the Nernst equation can only be used to estimate the electrode potential of the power source.

Cathodic reaction and its Nernst equation:



$$E(\text{Ag}^+|\text{Ag}) = E^\ominus(\text{Ag}^+|\text{Ag}) - \frac{RT}{F} \ln \frac{[\alpha(\text{Ag})]}{[\alpha(\text{Ag}^+)]} = 0.7994 \text{ V}$$

Anodic reaction and its Nernst equation:



$$E(\text{Al}(\text{OH})_3|\text{Al}) = E^\ominus(\text{Al}(\text{OH})_3|\text{Al}) - \frac{RT}{3F} \ln \frac{[\alpha(\text{Al})][a(\text{OH}^-)]^3}{[\alpha(\text{Al}(\text{OH})_3)]} = -2.31 \text{ V}$$

Where, E represents the standard electrode potential of this electrode. The activity of the solids $\alpha(\text{Ag})$, $\alpha(\text{Al})$ and $\alpha[\text{Al}(\text{OH})_3]$ is 1. In fact, the measured open-circuit voltage (V_{oc}) of the iontronic power source is much lower than the theoretical value, which may be due to the relatively high internal resistance of the power source.

Note S3: Power density and energy calculations for iontronic power sources.

Energy Materials

The device's power and energy output are evaluated by adjusting the external load resistance (R_L) of the iontronic power source using a ZX21g rotary resistor box. The voltage (U_R) and current (I_R) across the external load resistor R_L were measured by using a multi-channel electrochemical workstation Autolab, respectively. Therefore, the device's power density with the external load resistance R_L can be calculated using the following formulas:

$$P_A^R = U_R \times I_R \#(2)$$

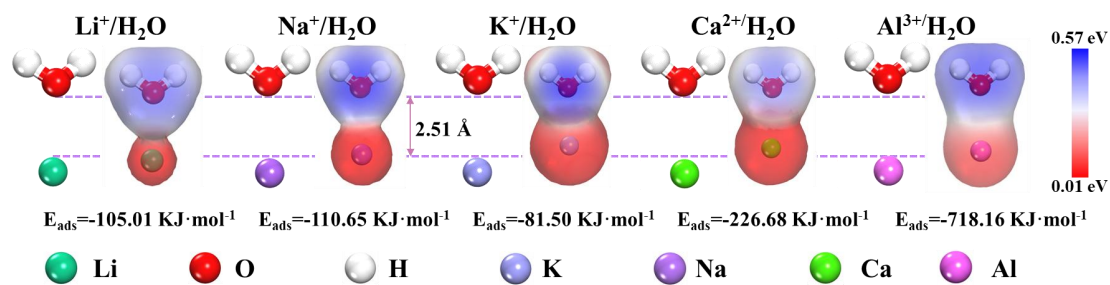


Figure S1. Desolvation energy barriers of different salt solution ions with water molecules.

Desolvation energy barriers for the fully hydrated metal cations Li⁺, Na⁺, K⁺, and Ca²⁺ were calculated using density functional theory (DFT). The desolvation energy barrier of an ion is defined by the following formula:

$$\Delta E_{ads} = E_{Total} - (E_{Host} + E_{H_2O}) \#(1)$$

Where E_{Total} represents the total energy of the system when the cation interacts with an H₂O molecule. The total energy of a single dehydrated metal cation is denoted as E_{Host} , while the standard energy of water is represented by as E_{H_2O} . The desolvation energy barrier of the system, with the ion positioned 2.51 Å from the H₂O molecule, is illustrated in **Figure S1**. The K⁺ cation exhibits the lowest desolvation energy barrier among the solution systems compared to the other three hydrated ions, which facilitates its release from the hydration shell, reducing polarization resistance when it enters into the two-dimensional nanofluidic channels. Consequently, K⁺, with its minimal desolvation energy barrier, was selected as the cation for diffusion within GO

2D nanofluidic channels.

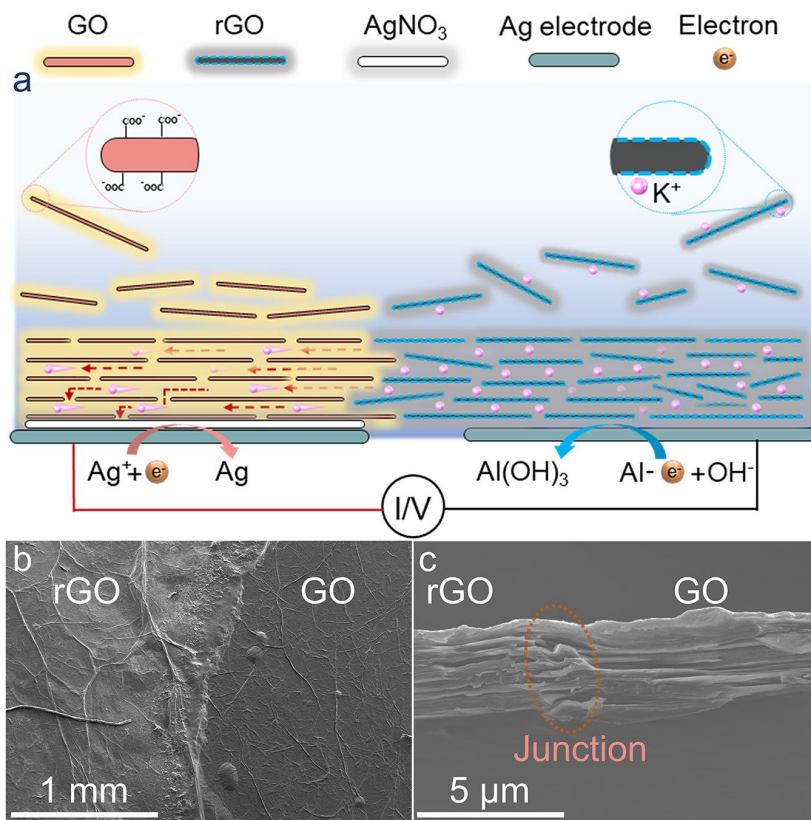


Figure S2. (a) Front view of the iontronic power source. (b) Top SEM image of the GO and rGO junction interface. (c) Cross-sectional SEM image of the GO and rGO junction interface.

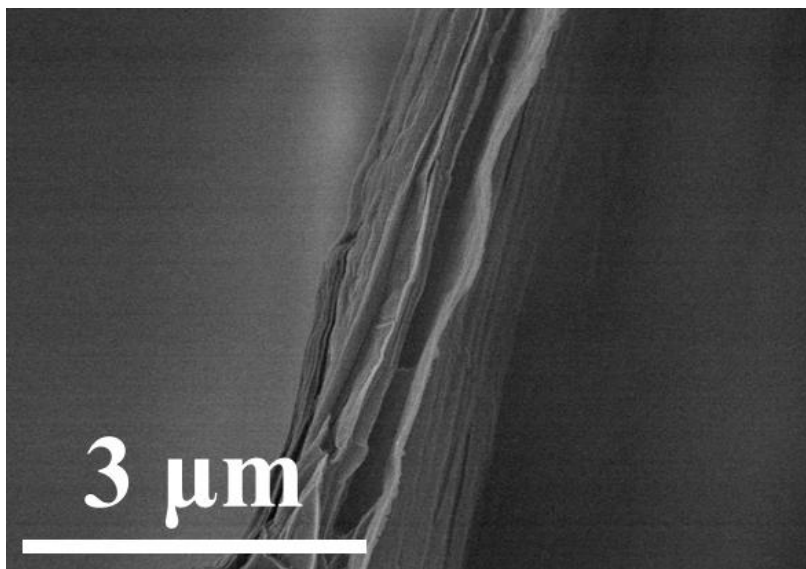


Figure S3. Scanning electron microscope image of graphene oxide.

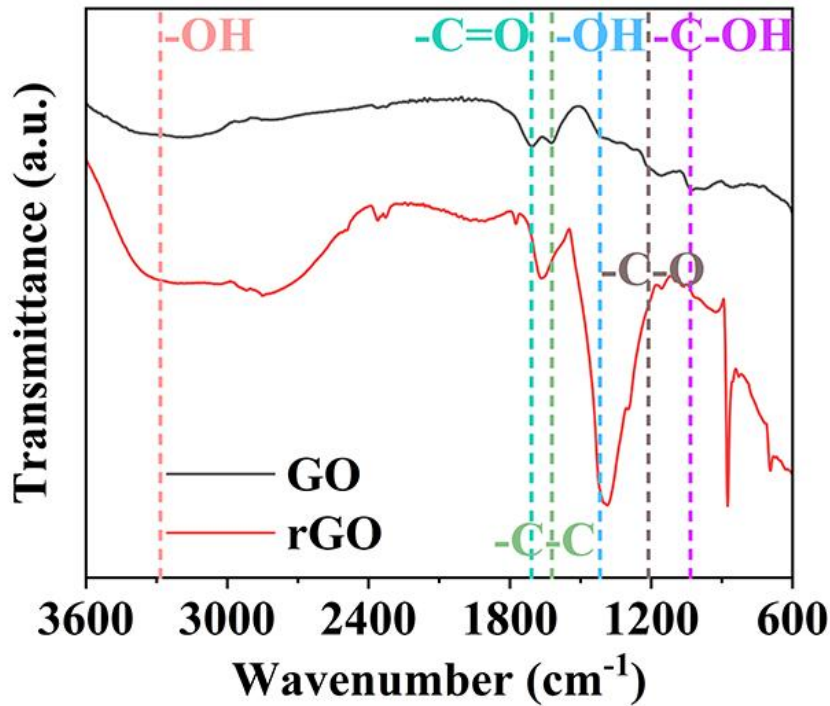


Figure S4. Fourier transform infrared spectroscopy (FTIR) for graphene oxide (GO). The surface of graphene oxide features -C=C bonds ($\sim 1618.1 \text{ cm}^{-1}$) and oxygen-containing functional groups, including C-O bonds ($\sim 1027.9 \text{ cm}^{-1}$), C-O-C bonds (epoxy groups, $\sim 1020.8 \text{ cm}^{-1}$), C-OH bonds ($\sim 1411.8 \text{ cm}^{-1}$), C=O bonds (carbonyl groups, $\sim 1708.8 \text{ cm}^{-1}$), and -OH bonds (hydroxyl groups, $\sim 3282.6 \text{ cm}^{-1}$).

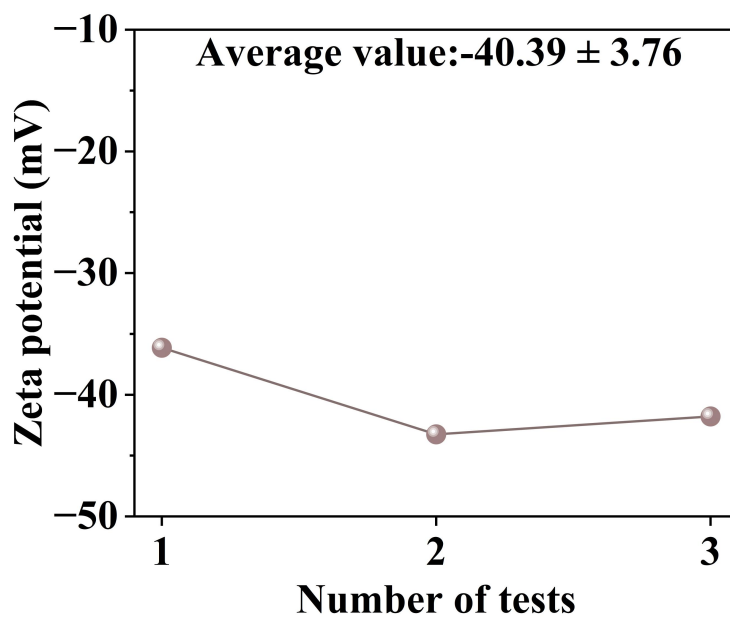


Figure S5. The zeta potential of GO.

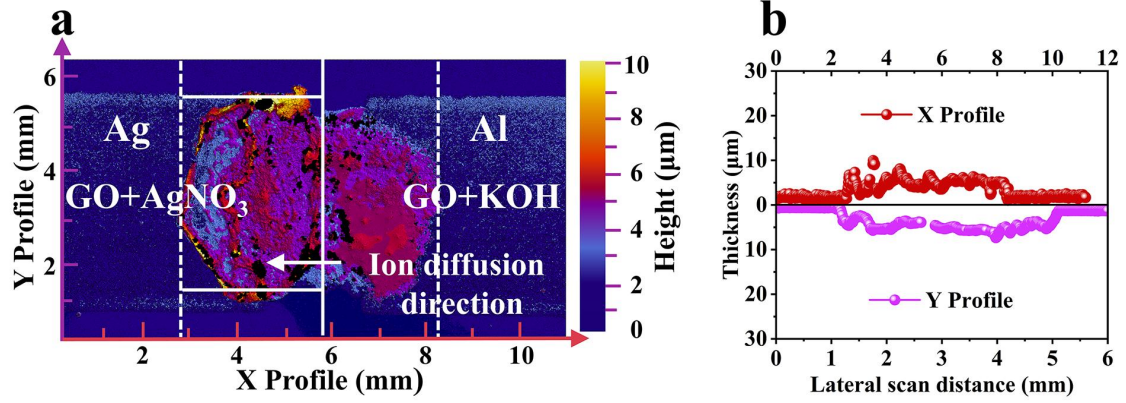


Figure S6. (a) The 3D surface profile of GO. (b) Numerical analysis of the length, width, and thickness of GO in the device.

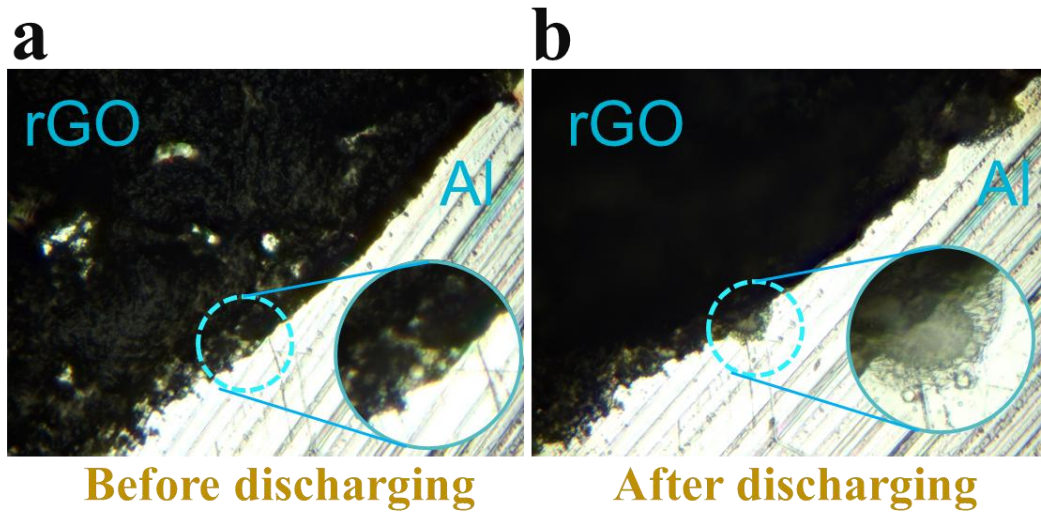


Figure S7 Optical photograph of the KOH/GO on the Al electrode (anode) side of the power source. (a) Optical microscopy image of the rGO side before discharge in the iontronic power source. (b) Optical microscopy image of the rGO side after discharge in the iontronic power source.

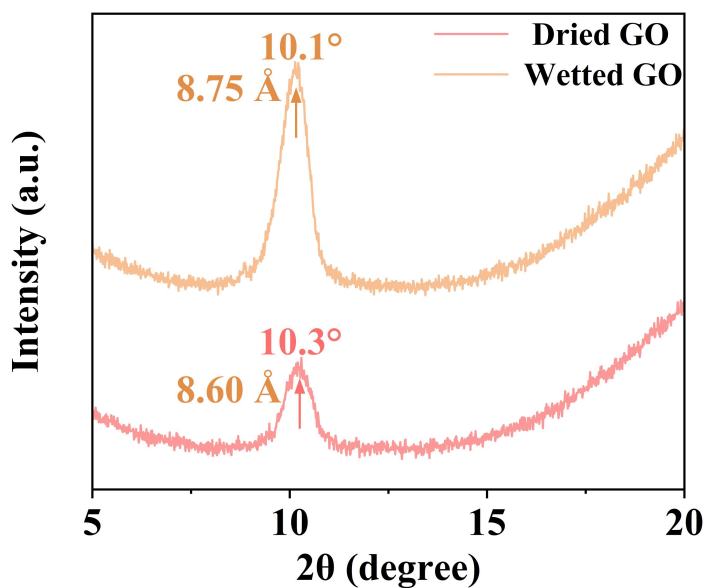


Figure S8. XRD spectra of the GO film before and after discharge of the ion-electronic power source system.

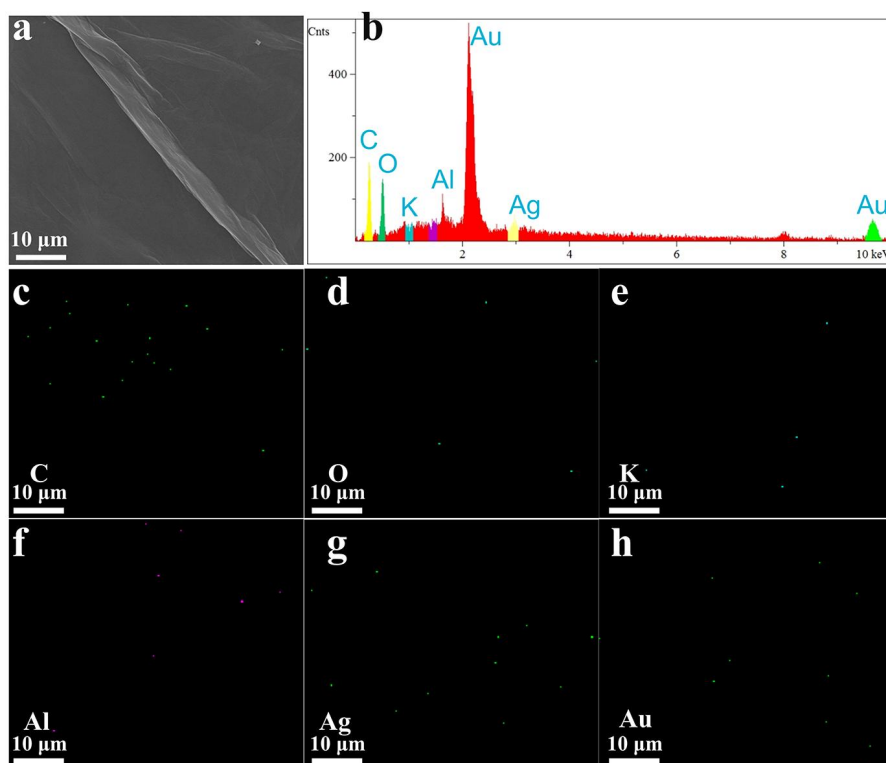


Figure S9 SEM and EDS images of GO/AgNO₃ on the Ag electrode (cathode) side **before discharging**. (a) SEM image of the GO on the cathode side. (b) The elemental composition within the GO on the cathode side. (c-h) EDS images of the various elements within the GO on the cathode side.

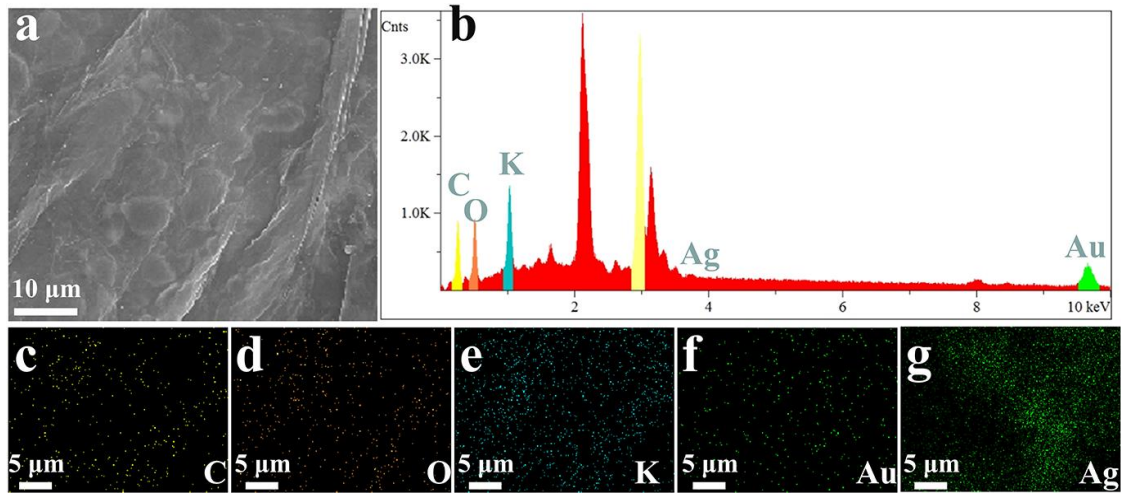


Figure S10 SEM and EDS images of GO/AgNO₃ on the Ag electrode (cathode) side after discharging. (a) SEM image of the iontronic power source's cathode side after discharge. (b) The elemental composition of the GO on the cathode side of the iontronic power source after discharge. (c-g) EDS images of the various elements within the GO on the cathode side after discharge.

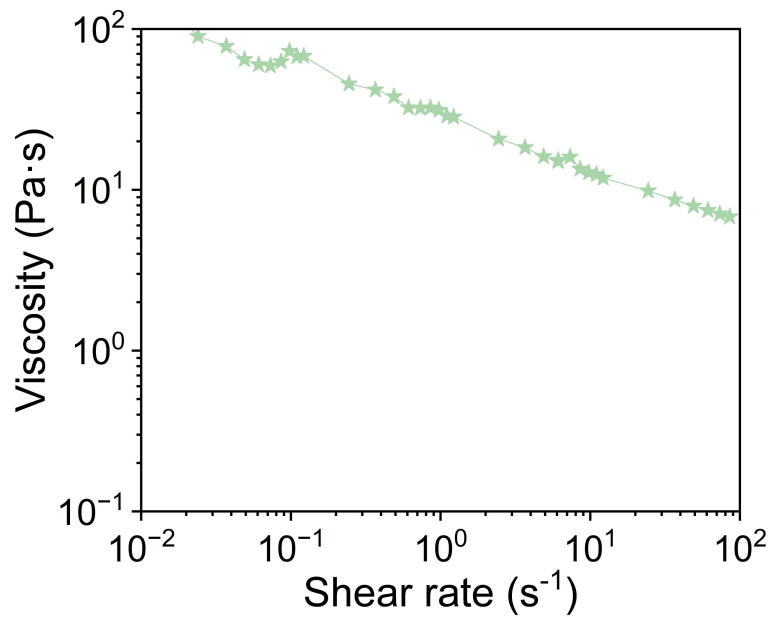


Figure S11 The relationship between the viscosity of GO ink and the shear rate.

Energy Materials

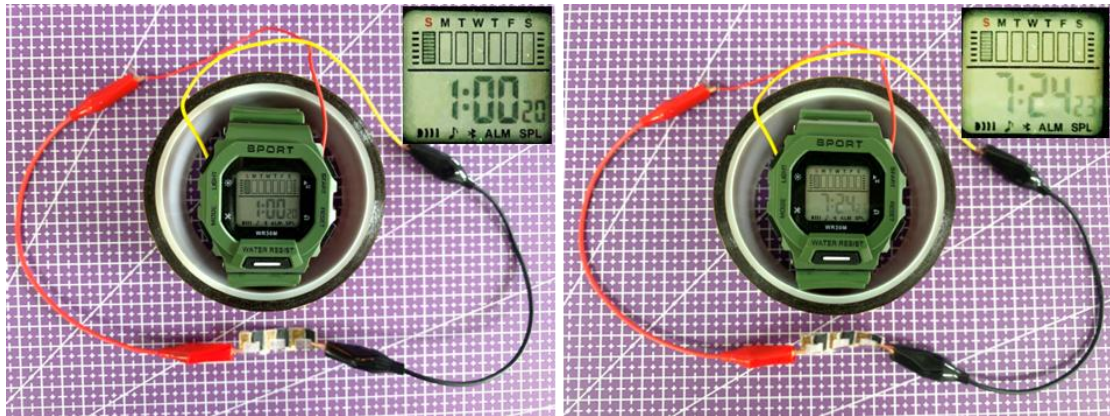


Figure S12 Three integrated devices can power a watch for over 6 h at 25°C and 45% RH.

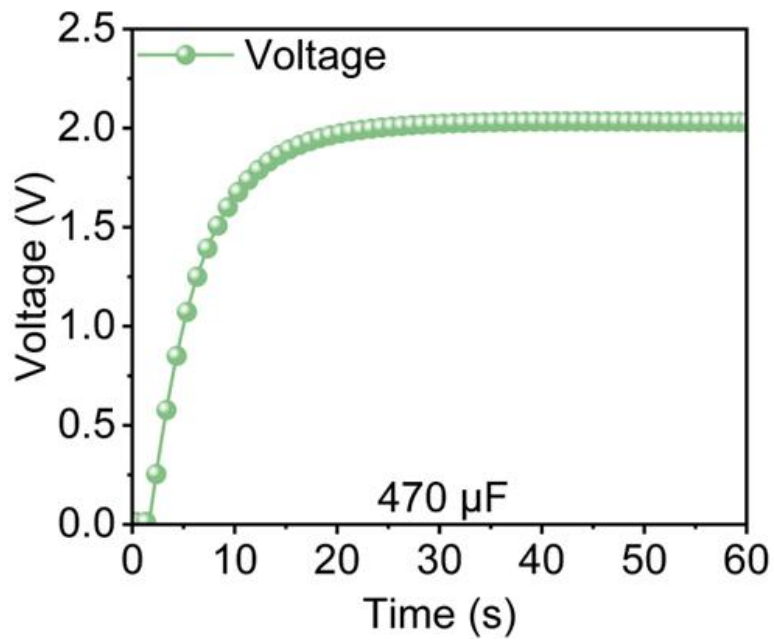


Figure S13 An iontronic power source charges a 470uF capacitor up to 2V.

Energy Materials

Table S1. Comparison of the performance outputs across various iontronic power sources

Type	Ref	Materials	Voltage (V)	Current density $\mu\text{A}\cdot\text{cm}^{-2}$
This Work		GO-AgNO ₃ /rGO	~2.0	2.35·10 ⁴
MEGs	[S1]	PDDA/SiNWs	1.0	8.2
	[S2]	PAN	0.8	14.3
	[S3]	GO/rGO	0.76	73.0
	[S4]	1T-WS ₂ @CSilk	0.65	170
	[S5]	H-PSS	0.80	120
WEGs	[S6]	MOFs	0.40	2.7
	[S7]	LiCl-Cellulon paper	0.78	0.8
	[S8]	SiNWs	0.40	55
	[S9]	Cellulon paper	0.71	700
	[S10]	SiNWs	1.50	0.40
Iontronic power source	[S11]	PEDOT-GO/rGO	0.70	1.30·10 ³

MEGs: Moist-electric generators

WEGs: Water evaporation-induced electric generators

Table S2. The proportion of various elements within the GO on the cathode side

Elt.	Line	Intensity (c/s)	Conc	Units	Error 2-sig	MDL 3-sig
C	Ka	92.09	34.800	wt.%	0.819	0.610
O	Ka	55.36	27.124	wt.%	1.304	0.924
K	Ka	3.47	0.580	wt.%	0.162	0.404

Energy Materials

Al	Ka	4.85	0.496	wt.%	0.121	0.259
Ag	La	13.60	2.721	wt.%	0.215	0.466
Au	La	24.96	34.278	wt.%	1.252	1.635
			100.000	wt.%		Total

Table S3. The proportion of various elements within the GO on the cathode side after discharge.

Elt.	Line	Intensity (c/s)	Conc	Units	Error 2-sig	MDL 3-sig
C	Ka	55.21	18.121	wt.%	0.574	0.482
O	Ka	36.13	16.722	wt.%	0.728	0.886
Na	Ka	50.58	7.463	wt.%	0.289	0.411
Ag	La	189.71	29.208	wt.%	0.470	0.635
Au	La	26.84	28.486	wt.%	1.128	1.576
			100.000	wt.%		Total

References

- [S1] Wu Y, Shao B, Song Z, et al. A Hygroscopic Janus Heterojunction for Continuous Moisture-Triggered Electricity Generators. *ACS Appl. Mater. Interfaces* **2022**; 14: 19569-19578. DOI: 10.1021/acsami.2c02878.
- [S2] Sun Z, Wen X, Guo S, et al. Weavable yarn-shaped moisture-induced electric generator. *Nano Energy* **2023**; 116: 108748. DOI: 10.1016/j.nanoen.2023.108748.
- [S3] Chen F, Zhang S, Guan P, et al. High-Performance Flexible Graphene Oxide-Based Moisture-Enabled Nanogenerator via Multilayer Heterojunction Engineering and Power Management System. *Small* **2024**; 20: 2304572. DOI: 10.1002/smll.202304572.
- [S4] Han B-B, Luo P, Xue Y-B, et al. Hydrophilic 1T-WS₂ Nanosheet Arrays toward Conductive Textiles for High-Efficient and Continuous Hydroelectric Generation and

- Storage. *Small* **2024**; 20: 2308527. DOI: 10.1002/sml.202308527.
- [S5] Huang Y, Zhou K, Cheng H, et al. Three-Dimensional Printing of High-Performance Moisture Power Generators. *Adv. Funct. Mater.* **2024**; 34: 2308620. DOI: 10.1002/adfm.202308620.
- [S6] Wang Z, Huang Y, Zhang T, et al. Unipolar Solution Flow in Calcium–Organic Frameworks for Seawater-Evaporation-Induced Electricity Generation. *J. Am. Chem. Soc.* **2024**; 146: 1690-1700. DOI: 10.1021/jacs.3c13159.
- [S7] Tan J, Fang S, Zhang Z, et al. Self-sustained electricity generator driven by the compatible integration of ambient moisture adsorption and evaporation. *Nat. Commun.* **2022**; 13: 3643. DOI: 10.1038/s41467-022-31221-7.
- [S8] Qin Y, Wang Y, Sun X, et al. Constant Electricity Generation in Nanostructured Silicon by Evaporation-Driven Water Flow. *Angew. Chem. Int. Ed.* **2020**; 59: 10619-10625. DOI: <https://doi.org/10.1002/anie.202002762>.
- [S9] Liu Y, Li Z, Wang, Liying, et al. Surface Functional Modification for Boosting Power Density of Hydrovoltaic Devices. *Adv. Funct. Mater.* **2024**; 34: 2312666. DOI: 10.1002/adfm.202312666.
- [S10] Shao B, Wu Y, Song Z, et al. Freestanding silicon nanowires mesh for efficient electricity generation from evaporation-induced water capillary flow. *Nano Energy* **2022**; 94: 106917. DOI: 10.1016/j.nanoen.2022.106917.
- [S11] Wei D. Writable electrochemical energy source based on graphene oxide. *Sci. Rep.* **2015**; 5: 15173. DOI: 10.1038/srep15173.